Paper No.
07556

NACE INTERNATIONAL CORROSION 2007 CONFERENCE & EXPO

A Mechanistic Model of Top of the Line Corrosion

Z. Zhang, D. Hinkson, M. Singer, H. Wang*, S. Nesic
Ohio University - Institute for Corrosion and Multiphase Technology
342 West State Street, Athens, OH 45701

ABSTRACT

A mechanistic model is developed to predict the general corrosion rate at the top of a gas pipeline. This model covers the three main processes involved in the Top of the Line Corrosion (TLC) phenomena: the dropwise condensation, the behavior of the chemistry in the condensed water and the corrosion at the steel surface. The dropwise condensation process is modeled based on the heat and mass transfer theory and is used to predict the condensation rate. The breakdown of species concentrations in the droplet is established through the main thermodynamic and chemical equilibrium. The general corrosion rate is predicted using the kinetics of the electrochemical reactions at the steel surface and by taking into account the mass transfer and chemical reactions occurring inside the droplet. Finally, the accuracy of the predictions of the model is evaluated by comparison with experimental data.

Keywords: top of the line corrosion, carbon dioxide, dropwise condensation, mechanistic model

INTRODUCTION

Top-of-the-Line Corrosion (TLC) is a phenomenon encountered in the oil and gas industry when problems of corrosion appear inside the pipe due to the condensation of water containing dissolved corrosive gases. TLC occurs exclusively in wet gas transportation and in a stratified flow regime. Condensation happens when the environment outside the pipeline is cooler than the saturated vapor flowing inside the pipe. The water vapor in the gas phase condenses on the pipe wall in two different ways:

- on the side walls of the pipe where the condensed liquid slides to the bottom of the line due to gravity forces;
- at the top of the pipe where droplets of liquid form and remain attached at the metal surface for a longer time.

The dissolution of corrosive gases, such as carbon dioxide (CO_2) and hydrogen sulfide (H_2S) as well as condensation of acidic vapors such as acetic acid (HAc) in the droplet can cause serious corrosion

* Current address: Clariant Corporation, Functional Chemicals Division, 8701 New Trails Drive, Suite 100, The Woodlands, Texas. USA 77381

problems at the metal surface. The top of the line is the most critical location since severe problems of localized corrosion can occur there. The injection of chemical inhibitors (a standard method to fight corrosion issues at the bottom of the line) is not effective as they cannot reach the top of the line easily. Top of the Line Corrosion has become a growing concern in the oil and gas industry and a better understanding of the corrosion mechanisms involved is needed. At the same time there are no predictive tools available for this type of corrosion and a mechanistic model presented below is devised to satisfy this need.

Since Estavoyer[1] reported a case of TLC in an oil field, much work has been done in this area. Olsen and Dugstad[2] conducted a study to look at some of the key parameters in TLC. In their study the effects of temperature and condensation rate on the formation of protective iron carbonate scale were investigated. Also an increase in gas flow rate was found to increase the condensation rate, which in turn influences the corrosion at the top of the line. However, Olsen and Dugstad did not propose a model or any correlation between corrosion and the parameters they studied. In 1993 de Waard[3] modified his corrosion model for the full pipe flow after introducing a correction factor to predict the corrosion rate at top of the line for condensation rates below a typical field value of 0.25 ml/m^2/s. From a TLC failure in the field, Gunaltun[4] gave a complete description of the TLC phenomena for the first time, forming a solid basis for future experimentation and modeling efforts. Pots and Hendriksen[5] proposed an iron supersaturation model to calculate the corrosion rate using the condensation rate and precipitation rate of iron carbonate as the two key concepts. However without being able to reliably predict the condensation regime, and by ignoring other important parameters, this corrosion model was far from satisfying the needs of the industry. Vitse[6, 7] proposed a quasi-mechanistic model to predict the corrosion rate in TLC, however, all these efforts could be useful at best in describing corrosion during the filmwise condensation process, which is not common for the top of the line.

For better modeling of TLC it is necessary to have an accurate prediction of the condensation rate and the condensation regime. In the previous work many researchers tried to predict the condensation rate by using the filmwise condensation theory. However, large discrepancies arise when this theory is used to predict the condensation rate for the dropwise condensation process. In addition it is essential to be able to predict the water composition in the droplets as well as any iron carbonate scale formation with time.

In this work, a mechanistic condensation model will be established based on the dropwise condensation theory. This condensation model will predict droplet growth rate, which is a function of time. The chemistry inside the droplet is determined from the thermodynamic equilibrium at the liquid/gas interface and the electrochemical reactions at metal surface linked to the corrosion process. The mechanistic corrosion model presented by Nesic *et al*.[8 - 10] is used as a basis for all calculations and is combined with the dropwise condensation model to predict TLC phenomena. Finally, this model is verified through comparison between experimental data and predicted results.

CONDENSATION MODEL

When the condensed liquid cannot wet the wall surface completely, a discontinuous film of liquid can form on the metal surface. The dropwise condensation process at the top of line in wet gas conditions is one type of heterogeneous condensation, in which liquid embryos first nucleate at the interface between a metastable saturated vapor and another solid phase. The size of the droplet will increase as the vapor continuously condenses on the gas-liquid interface. Coalescence happens when adjacent droplets contact each other due to the continuous increase in droplet size. Therefore, the size of the water droplet would increase by means of either direct condensation of vapor or coalescence among adjacent droplets. As the droplet size increases at high gas velocity, the droplet might start to move along in the gas flow direction

as a result of drag forces from the motion of the surrounding gas, continuously sweeping other droplets on its way ahead. On the other hand, when a single droplet reaches its maximum size, it may flow down along the inner surface of the pipe wall as a result of gravity pull. In most situations a combined movement (forward and down) is seen. At very low gas velocity and very large pipe diameters the droplets may detach from the top pipe surface and fall to the bottom. New liquid embryos will form on the locations where the old droplets were removed and the cycle of nucleation, growth, moving/falling will repeat.

Dropwise condensation which happens at high concentration of non-condensable gas and low gas velocity was frequently observed in the laboratory tests and the industrial cases. Factors that will influence the condensation rate in the wet gas pipeline include:

- Gas temperature;
- Subcooling temperature (defined as $\Delta T = T_b^g - T_i^w$) where T_b^g is bulk gas temperature and T_i^w is inner wall temperature;
- Non-condensable gas concentration;
- Gas velocity;
- System pressure;
- Internal pipe diameter.

Since liquid nucleation of embryos in dropwise condensation is a random process, a statistical method (droplet size distribution function) is employed to model the overall heat transfer process. In order to calculate the condensation rate for dropwise condensation, two crucial parameters must first be obtained: droplet size distribution and heat transfer rate through each droplet of a given radius, *r*.

Droplet-size distribution function

At any given time, a family of droplets with different diameters occupies the pipe inner surface. This is called the *droplet-size distribution* in dropwise condensation. Equation (1) was first proposed by Rose[11] and is one of the most commonly used droplet-size distribution functions.

$$N(r)dr = \frac{n}{\pi r^2 r_{max}} \left(\frac{r}{r_{max}} \right)^{n-1} dr \qquad (1)$$

where:

$N(r)dr$	number of droplets at radius, *r*, over 1 m^2 surface area
n	exponent constant, typically as 1/3
r_{max}	the maximum droplet radius, m

Heat flux in dropwise condensation

The overall heat transfer process in dropwise condensation should take into account several crucial phenomena[12 - 14], as shown in Figure 1:

1) Heat transfer resistance in the gas phase boundary layer.
2) Water vapor condensation at the droplet surface.
3) The influence of droplet surface curvature on the phase equilibrium temperature. This is important especially for small droplets.

4) Vapor-liquid interfacial resistance. In the condensation process only part of the vapor molecules which are striking the liquid surface can enter the liquid phase. This causes a thermal resistance to heat transfer.
5) Heat conduction resistance through the droplets. It is important to point out that the heat conduction resistance is not uniform through a droplet since the distance from the droplet surface (gas-liquid interface) to the inner pipe wall changes from the apex to the drop base perimeter (gas-liquid-solid three phase interface).
6) Heat conduction resistance through the pipe wall and the insulation layer to the environment.

Heat balance

Due to the fact that the heat transfer resistance in the gas phase is significant when non-condensable gases are present and that the phase change (vapor condensation) happens at the interface, the total flux of heat Q between the gas phase and the droplets can be written as:

$$Q = Q_g + Q_c \qquad (2)$$

where:

Q_g heat flux through the gas boundary layer to the droplet surface, W/m^2
Q_c latent heat flux released by the phase change at the droplet surface, W/m^2

1) For a fully developed gas boundary layer the heat flux Q_g can be calculated by:

$$Q_g = h_g \cdot \left(T_b^g - T_i^g\right) \qquad (3)$$

where:

h_g heat transfer coefficient for the gas boundary layer, W/m^2 /K
T_b^g temperature of the bulk gas, K
T_i^g temperature of the gas at the droplet interface, K

Here the heat transfer coefficient of the gas boundary layer in a pipeline can be estimated by empirical correlations (Dittus)[15].

$$Nu = 0.023 Re^{0.8} Pr^{0.4} \qquad (4)$$

where:

Nu	$= \mathrm{h_g} d / k_g$	Nusselt number
Re	$= \mathrm{v_g} d \rho_g / \mu$	Reynolds number
Pr	$= \hat{\mathrm{C}}_\mathrm{p} \mu / k_g$	Prantl number
d		internal pipeline diameter, m
$\mathrm{k_g}$		thermal conductivity of the gas, W/m·K
$\mathrm{v_g}$		the gas velocity, m/s

ρ_g the gas density, kg/m^3
μ the gas viscosity, Pa·s
$\hat{C}_p$ the heat capacity of the gas, J/K·kg

2) The latent heat flux is related to the condensation rate:

$$Q_c = \dot{m}\, H_{fg} \qquad (5)$$

where:

$\dot{m}$ condensation rate, kg$_g$/m^2/s
H_{fg} latent heat of evaporation/condensation for water, J/kg

The total heat flux between the gas phase and the droplets becomes:

$$Q = h_g \cdot \left(T_b^g - T_i^g\right) + \dot{m} H_{fg} \qquad (6)$$

To calculate the condensation rate $\dot{m}$ from this equation one needs to know the heat flux Q and find the unknown temperature of the gas at the interface with the droplets T_i^g by considering that the heat transferred from the gas to the droplets, passes through the droplets and the pipe wall to the outside environment.

3) The temperature drop ΔT_c at the droplet interface due to droplet curvature is defined as[13]:

$$\Delta T_c = \frac{2 T_i^g \sigma}{H_{fg} r \rho} \qquad (7)$$

where:

r radius of the droplet, m
σ vapor-liquid surface tension, N/m
ρ water density, kg/m^3

4) The amount of heat q in W, carried through the interface of a droplet with a radius r is [13]:

$$q(r) = 2\pi r^2 h_i \left(T_i^g - T_i^d\right) = 2\pi r^2 h_i \Delta T_i \qquad (8)$$

where

h_i heat transfer coefficient at the droplet interface, W/m^2/K
T_i^d temperature of the droplet at the interface with the gas, K
ΔT_i temperature drop due to vapor-liquid interfacial resistance for a hemispherical droplet, K

5) Then the heat is conducted through the bulk of the droplet [12]:

$$q(r) = \frac{4\pi r^2 k_{H_2O}}{r}\left(T_i^d - T_i^w\right) = 4\pi r k_{H_2O}\Delta T_d \qquad (9)$$

where

k_{H_2O} thermal conductivity of the water, W/m/K

T_i^w temperature of the droplet at the interface with the pipe wall, K

ΔT_d temperature drop due to heat conduction through a hemispherical droplet, K

6) Finally the heat exits through the pipe wall out to the environment:

$$q(r) = \frac{4\pi r^2 k_w}{d_w}\left(T_i^w - T_o^w\right) = \frac{4\pi r^2 k_w}{d_w}\Delta T_w \qquad (10)$$

where:

k_w thermal conductivity of the steel pipe wall, W/m/K

d_w thickness of pipe wall, m

T_o^w temperature of the outer pipe wall, K

ΔT_w temperature drop due to heat conduction through the cylindrical pipe wall, K

One can write the overall temperature difference between the surface of the droplet T_i^g and the outer pipeline wall T_o^w as:

$$T_i^g - T_o^w = \Delta T_c + \Delta T_i + \Delta T_d + \Delta T_w \qquad (11)$$

By substituting the various ΔT from equations (7) - (10) into equation (11), the amount of heat $q(r)$ transferred through a droplet of radius *r* can be expressed as:

$$q(r) = \frac{T_i^g\left(1 - \dfrac{2\sigma}{H_{fg} r \rho}\right) - T_o^w}{\dfrac{r}{4\pi r^2 k_{H_2O}} + \dfrac{1}{2\pi r^2 h_i} + \dfrac{d_w}{4\pi r^2 k_w}} \qquad (12)$$

The total heat flux for a unit area of the pipe wall covered by a large number of droplets of various sizes can be calculated by summing all the fluxes, which can be written as [12]:

$$Q = \int_{r_{min}}^{r_{max}} q(r)N(r)dr \qquad (13)$$

where:

r_{max} maximum radii of droplet, m

r_{min} minimum radii of droplet, m

There are two flux equations (6) and (13) and three unknowns, Q, T_i^g and $\dot{m}$. Writing the mass balance closes the system and enables the calculation of the condensation rate $\dot{m}$ for the case of dropwise condensation.

Mass balance

All the water condensing at the pipe wall comes from the gas phase, i.e. the water vapor needs to pass through the mass transfer boundary layer to get to the wall. Therefore one can equate the condensation rate to the mass flux of water through the gas phase. When non-condensable gases are present, the resistance to mass transfer of water vapor in the boundary layer can be rather significant. This makes the heat and mass transfer coupled and therefore they have to be solved simultaneously. One can write:

$$\dot{m} = \rho_g \beta_g (x_b^g - x_i^g) \qquad (14)$$

where:

β_g mass transfer coefficient in the gas boundary layer, m/s

x_b^g mass fraction of water vapor in the bulk gas flow, kg_v/kg_g

x_i^g mass fraction of water vapor at the gas-liquid interface, kg_v/kg_g

ρ_g density of gas, kg_g/m^3

The mass transfer coefficient for the gas boundary layer can be estimated using the analogy [16] between heat and mass transfer, according to

$$\rho_g \beta_g = \frac{h_g}{\hat{C}_p} Le^{2/3} \qquad (15)$$

where:

$Le = k_g / \rho_g \hat{C}_p D_v$ Lewis number

D_v diffusivity of water vapor in the gas phase, m^2/s

The mass fraction of water vapor in a saturated gas mixture $x(T)$ is a function of temperature T and can be calculated according to:

$$x(T) = \frac{p_{sat}(T)}{p_{tot}} \qquad (16)$$

where:

$p_{sat}(T)$ saturation vapor pressure as a function of temperature, kPa

p_{tot} total pressure, kPa

Therefore this constitutes another way that the heat and mass transfer processes are coupled:

$$x_b^g = x(T_b^g) = \frac{p_{sat}\left(T_b^g\right)}{p_{tot}} \qquad (17)$$

$$x_i^g = x(T_i^g) = \frac{p_{sat}\left(T_i^g\right)}{p_{tot}} \qquad (18)$$

To be able to solve the set of coupled heat and mass equations (6), (13) and (14) and obtain the condensation rate, one needs to know the minimum and maximum size of the droplets that are found on a condensing steel surface.

Determination of minimum and maximum radii of droplets

Minimum radius[14]: The saturation temperature and pressure in equilibrium are slightly dependent on the shape of the interface between the gas and the liquid. The difference of saturation temperature between curved surface and flat surface is thought of as the minimum driving force (i.e. subcooling temperature) to form a droplet on the solid surface. Using Clapyron relation and the equation of equilibrium on curved surface, the minimum droplets can be calculated for a given wall subcooling through:

$$r_{\min} = \frac{2T_s\sigma}{H_{fg}\rho\Delta T} \qquad (19)$$

Maximum radius: It is well known that gas velocity has a great influence on TLC. On one hand it affects the heat and mass transfer in the gas boundary layer (see equations (3) and (14)), which are some of the most important steps in the whole condensation process. On the other hand the drag force exerted by the flowing gas onto the droplets is the key factor for determining droplet size and motion at the top of the line. Through an analysis of the forces acting on a suspended droplet, it is possible to gain some insight into the mechanics of droplet growth and motion. In Figure 2, forces are considered as acting on a single hemispherical suspended droplet at the top of the line.

- The drag force F_D^x represents the pull by the flowing gas exerted on the droplet. It can be expressed [(17)] by:

$$F_D^x = \frac{1}{2} C_D \ \rho_g \ A \ v_g^{\,2} \qquad (20)$$

where:

C_D	drag coefficient
$A = r^2\pi / 2$	frontal area of the droplet, m^2
v_g	gas velocity, m/s

The drag coefficient C_D depends on the shape of the droplet. In turbulent flow, C_D is equal to 0.44 for hemispherical droplets.

- The "friction" force F_f^x represents the adhesion between droplet and the steel wall that opposes the drag force and keeps the droplet in place. For a suspended droplet, an empirical equation is adopted from Bikerman[18]:

$$F_f^x = k_f \cdot \sigma \cdot r \qquad (21)$$

where:

σ surface tension, N/m

k_f friction coefficient which is a function of inner pipe surface roughness h:

$$k_f = f(h) \qquad (22)$$

Bikerman[19] performed a series of experiments on the surface of steel to determine the effect of surface roughness on the sliding droplets. It was found that when h is less than 0.5 μm the coefficient k_f changes significantly with roughness. But when h is is in the range 0.5 to 3.0 μm, the coefficient k_f is approximately constant around 1.5.

- Gravity force F_g^y tends to either detach the droplet from the top of the pipe or cause it to slide down the sides of the pipe:

$$F_g^y = \rho \frac{4}{6} \pi r^3 g \qquad (23)$$

- The downward drag force F_D^y arises due to the hemispherical shape of the droplets. No explicit expressions for calculation of this force have been found and in this study it is assumed:

$$F_D^y = \frac{1}{2} F_D^x \qquad (24)$$

- The surface tension force F_σ^y keeps the droplet attached to the pipe wall and counters the effect of gravity. For a hemispherical droplet it (Davies)[20] can be calculated as:

$$F_\sigma^y = \pi r^2 \frac{2\sigma}{r} \qquad (25)$$

- The buoyancy F_B^y for a suspended hemispherical droplet can be calculated as:

$$F_B^y = \frac{4}{6} \pi r^3 \rho_g \qquad (26)$$

where:

ρ_g gas density, kg/m^3

Very small droplets are firmly attached to the steel surface i.e. the friction force is much larger than the drag force: $F_f^x > F_D^x$ and the droplet cannot slide along the pipe wall. Also, the surface tension and the pressure forces exceed the gravity and downward drag forces: $F_\sigma^y + F_B^y > F_g^y + F_D^y$ so the droplet does not detach and fall. Clearly all the forces are a function of the droplet diameter. As condensation proceeds and a droplet grows the effect of gravity increases fastest (with r^3). When the droplet reaches a critical size, a force balance in either x direction or y direction is reached. If the force balance in y direction is established before that in x direction, the droplet will fall down before it slides away. If the force balance in x direction is established before that in y direction, the droplet will slide along the pipe before it detaches and falls down. In either case, this represents the lifetime of a single droplet and the maximum radius r_{max} of the droplet can be calculated.

Verification of the condensation model

With the model described above, the condensation rate for a dropwise regime can be calculated for a wide range of experimental conditions. In order to verify the model some experiments have been performed in large scale, high temperature, high pressure flow loops. The test section (Figure 3) where the data were collected was equipped with cooling system, from which the condensed liquid was collected for measurement of condensation rate. The comparison between experiments and model prediction are shown in Figure 4. The condensation model gives a good prediction of condensation rate.

In a separate series of experiments, the lifetime of droplets suspended at the top of the pipe and exposed to gas flow was studied by using video recording. The measured maximum size of droplet is compared with the predictions in Figure 5 and very good agreement is achieved. Note how under the given set of conditions, the droplet lifetime ends due to dislodgement by gravity at low velocities while at high velocity this happens due to gas drag force.

CORROSION MODEL

Before being dislodged, a condensed droplet remains attached to the metal surface for a long time, growing gradually. In order to simplify the mathematical challenge in describing this, the two-dimensional hemispherical droplet is represented with a one-dimensional column of liquid (as shown in Figure 6). Droplet growth due to condensation is represented by the increase in the height of the water column until the maximum size of the droplet r_{max} is reached. At that point the droplet is dislodged and new droplet starts growing in its place; this is simulated by reducing the size of the water column to r_{min} and the cycle starts all over again.

The corrosion at the top of the line (or anywhere else for that matter) involves three important processes occurring simultaneously:

- chemical reactions, including homogeneous (dissociation, dissolution, etc.) and heterogeneous (precipitation of corrosion product scales),
- electrochemical reactions at the metal surface and
- transport of species in the liquid droplet.

Since these processes occur at different velocity, the slowest one will be the rate controlling process which will determine the corrosion behavior. These processes are modeled according to the physics underlying the different phenomena. Fundamental equations, already published in Nesic work [8-10], are used to quantify the whole process mathematically. All constants in the equation system, such as equilibrium constants, reaction rate constants and diffusion coefficients, are taken from the open literature referenced by Nesic's papers [8-10].

Chemical reactions

Water dissociation	$H_2O \Leftrightarrow H^+ + OH^-$
Dissolution of carbon dioxide	$CO_2\,(g) \Leftrightarrow CO_2\,(l)$
Carbon dioxide hydration	$CO_2 + H_2O \Leftrightarrow H_2CO_3$
Carbonic acid dissociation	$H_2CO_3 \Leftrightarrow H^+ + HCO_3^-$
Bicarbonate anion dissociation	$HCO_3^- \Leftrightarrow H^+ + CO_3^{2-}$
Acetic acid Liquid / vapor equilibrium	$HAc\,(l) \Leftrightarrow HAc\,(vap)$
Acetic acid dissociation	$HAc \Leftrightarrow H^+ + Ac^-$

All the reactions shown above can be in equilibrium if the reaction rates are fast compared to other processes in the corroding system. Generally, for any set of k chemical reactions involving j species one can write compactly:

$$R_j = a_{jk}\Re_k \qquad (27)$$

where tensor notation applies for the subscripts, a_{jk} is the stoichiometric matrix where row j represents the j-th species, column k represents the k-th chemical reaction, and $\Re_k$ is the reaction rate vector. Using this technique any number of homogenous chemical reactions can be added to the model with little effort.

Transport processes

In the droplets, the transport of species can be described using a species conservation equation. The expression for transport of species i in the presence of chemical reactions is valid for the pure liquid in the droplet as well as for the liquid in the porous surface scale:

$$\frac{\partial \varepsilon C_i}{\partial t} = -\frac{\partial\left(\kappa N_i\right)}{\partial y} + \varepsilon R_i \qquad (28)$$

where:

C_i	concentration of species i, moles/m^3
ε and κ	volumetric porosity and surface permeability of the scale respectively (both equal to unity outside the corrosion product layer),
N_i	flux of species i, moles/m^2·s
R_i	source or sink of species i due to chemical reaction, moles/m^3·s
t	time, s
y	spatial coordinate.

The transport of species has three components: diffusion, convection and electromigration. In the first approximation it can be assumed that the liquid in the droplets is stagnant, and therefore no convection term exists in the species conservation equation. The electromigration is neglected as well and the electroneutrality equation is used instead:

$$\sum_i z_i \cdot C_i = 0 \qquad (29)$$

where:

z_i number of charge for species i,

Therefore, the flux contains only a diffusion term and can be expressed using Fick's law:

$$N_i = -D_i \cdot \frac{\partial C_i}{\partial y} \qquad (30)$$

where:

D_i molecular diffusivity of species i, m^2/s

Combining all equations above, the overall species conservation equation in the droplet becomes:

$$\frac{\partial \varepsilon C_i}{\partial t} = D_i \frac{\partial^2 \left(\kappa C_i\right)}{\partial y^2} + \varepsilon R_i \qquad (31)$$

The permeability κ of surface scales for transport of species depends on the amount of pores in the scale and the shape and connections between the pores (expressed via the tortuosity factor). If one assumes that the superficial porosity is approximately equal to the volumetric porosity and that the tortuosity is proportional to a square root of the porosity (what is typically the case for mineral scales), the permeability of surface scales for transport of species can be found as $\kappa = \varepsilon^{1.5}$.

Scale growth

The calculation of the porosity ε and the overall scale growth model is taken entirely from Nesic's paper [10]. For $FeCO_3$, there is an additional species conservation equation written in the same form as for other species (with the diffusion term neglected as $FeCO_3$ is a solid).

$$\frac{\partial C_{FeCO_3}}{\partial t} = R_{FeCO_3} \qquad (32)$$

The volumetric porosity ε describes the morphology of the $FeCO_3$ scales and is the principal scale parameter affecting the transport of species.

$$\varepsilon = \frac{V_{void}}{V_{total}} = \frac{\left(V_{total} - V_{FeCO_3}\right)}{V_{total}} = 1 - \frac{V_{FeCO_3}}{V_{total}} = 1 - \frac{C_{FeCO_3} \cdot M_{FeCO_3}}{\rho_{FeCO_3}} \qquad (33)$$

where:

M_{FeCO3} iron carbonate's molecular weight (115.8 kg/mol)

ρ_{FeCO3} iron carbonate's density (3.9 kg/m^3)

The scale growth equation (32) can be then expressed as a function of porosity:

$$\frac{\partial \varepsilon}{\partial t} = -\frac{M_{FeCO_3}}{\rho_{FeCO_3}} R_{FeCO_3} \qquad (34)$$

The $FeCO_3$ precipitation/dissolution reaction is modeled using Van Hunnik's [21] equation:

$$R_{FeCO_3} = \frac{A}{V} \cdot e^{52.4 - \frac{119.8}{RT}} \cdot K_{sp} \cdot (S-1) \cdot (1 - S^{-1}) \qquad (35)$$

where:

K_{sp} solubility product for iron carbonate, (moles/m^3)^2

S supersaturation ($S = \frac{C_{Fe^{2+}} \cdot C_{CO_3^{2-}}}{K_{sp}}$)

The surface to volume ratio A/V for the porous scale is calculated locally throughout the porous scale as:

$$\frac{A}{V} = \frac{\varepsilon^2 \cdot (1-\varepsilon)}{\Delta x} \qquad (36)$$

where:

Δx width of the control volume, m

Initial and boundary conditions

Initial conditions. Uniform concentrations of species as determined by chemical equilibria are used as initial conditions for all species.

Boundary conditions. On the outer boundary of the droplet, which is in contact with the gas, the boundary conditions are different for different species. For "volatile" species including CO_2, HAc and H_2S, the concentrations (C_i) are held constant as calculated by Henry's law:

$$C_i = H_i p_i \qquad (37)$$

where:

H_i Henry's law constant for species i,

p_i: partial pressure of species i in gas phase, kPa

For other species found only in the liquid phase a zero flux boundary condition is imposed at the droplet outer boundary.

At the metal surface, zero flux is specified for the species not involved in the electrochemical reactions. A number of electrochemical reactions are happening at the metal surface:

Cathodic reactions:

Hydrogen reduction	$2\ H^+ + 2\ e^- \rightarrow H_2$
Direct reduction of carbonic acid	$2\ H_2CO_3 + 2\ e^- \rightarrow H_2 + 2\ HCO_3^-$
Water reduction	$2\ H_2O + 2\ e^- \rightarrow H_2 + 2\ OH^-$

Anodic reactions:

Electrochemical dissolution of iron	$Fe \rightarrow Fe^{2+} + 2\ e^-$

For species j involved in electrochemical reactions at the metal surface, the flux at the metal surface can be determined from:

$$N_i = -\frac{i_i}{n_i F} \qquad (38)$$

where:

i_i partial current for species i, A/m^2

n_i number of mols of electrons exchanged per mol of species i

Fundamental rate equations of electrochemistry relate the current density i to the potential at the metal surface E via an exponential relationship:

$$i = \pm i_0 \cdot 10^{\pm\frac{E-E_{rev}}{b}} \qquad (39)$$

where

i_0 exchange current density, A/m^2

E_{rev} reversible potential, V

b Tafel slope, V

For a spontaneous corrosion process the unknown electrochemical potential at the metal surface E can be found from the charge balance equation at the metal surface:

$$\sum_1^{n_a} i_a = \sum_1^{nc} i_c \qquad (40)$$

n_a and n_c are the total number of anodic and cathodic reactions respectively.

Numerical methods

Since all equations are strongly and nonlinearly coupled through the chemical reaction term, they have to be solved simultaneously, together with the boundary conditions and initial conditions. The species conservation equations and the scale growth equation are discretized using a finite difference method and a non-uniform grid. A fully implicit time discretization scheme is used here for reasons of stability, and all nonlinear terms are linearized in variable space.

Most of the equations and techniques described above for the corrosion model are the same as proposed originally by Nordsveen, Nesic and Nyborg [9]. However, the domain of calculation had to be adapted to the TLC scenario in order to take into account the growth and demise of droplets with time.

The growth of the droplet is simulated by controlling (moving) the position of the liquid/vapor interface i.e. the outer boundary of the droplet. In reality, when the droplet reaches its maximum size and is removed from the top of the line, some liquid remains. This is even more true in the presence of porous corrosion product scales which hold water in the pores much like a sponge. This effect is included in the model. At the very beginning of the calculation when a first droplet with a minimum radius is generated, the initial concentrations in the droplet are set by equilibria for pure freshly condensed water. When this droplet grows the outer boundary of the computational domain is extended. When the droplet detaches, the computational domain is shrunk back to match the initial (minimum) droplet size while the concentrations of species in that small droplet are unchanged from what they were before detachment. The same is true if there is a corrosion scale, the species concentrations in the porous scale are retained after droplet detachment. The new freshly condensed droplet starts its lifetime on the outer side of the existing scale, i.e. the computational domain has the initial thickness equal to thickness of scale plus minimum droplet size.

Model verification

From Figure 7 which shows a typical simulation result at specific conditions, it can be seen that the corrosion rate at the very beginning is very high because the fresh condensation water is very corrosive. The corrosion rate, however, decreases dramatically as the protective scale forms on the metal surface in the first day. As the scale grows and becomes denser, the corrosion rate is further decreased and remains at a very low "steady state" value in long exposure. The jagged appearance of the corrosion rate curve is due to the many droplets that form, grow and detach during the course of the simulation, each "fluctuation" representing a single droplet's lifetime. Clearly when a new freshly condensed droplet forms the corrosion rate increases temporarily and then rapidly decreases as the droplet saturates with iron carbonate leading to a pH increase.

In most of TLC cases, the general corrosion rate is expected to decrease rapidly to a very small value since the chemistry in the droplets is ideal for the formation of protective corrosion product scale (small liquid volume, large corrosion rate leading to rapid iron carbonate supersaturation). From Figure 8 it follows that even at low gas temperature (40 °C), the formation of the corrosion scale still retards the corrosion rate dramatically. In the simulation, it is found that both the concentration of iron ions and pH are always very high. For example at these conditions (Figure 8) the pH in fresh condensed water is pH3.8, which is also the boundary condition at the interface of the droplets. But at the metal surface the iron ion concentration builds up due to corrosion and can be as high as 600 ppm (w/w). Due to the corrosion process the pH increases and rapidly reaches pH6.3, which leads to rapid protective film formation.

Several large-scale flow loops have been built at the Institute for Corrosion and Multiphase Technology to try to simulate as closely as possible the real field conditions. The description of these loops and the results are given in detail in other publications[22, 23]. The parameters, which are covered in the experiments discussed below, are shown in Table 1. All the experiments were conducted over long periods of time, up to three weeks, with weight loss coupons collected during the 2nd, 7th, 14th and 21st day of exposure. The influence of several parameters including gas temperature, gas velocity, CO_2 partial pressure, condensation rate and HAc concentration were investigated. The comparison between experimental data and predicted results in Figure 9 show a satisfactory agreement. In the simulation the

model slightly overpredicts the corrosion rates for short term experiments (2 days), which makes some points in this graph deviate from the diagonal line.

CONCLUSIONS

- A mechanistic model has been developed, which includes dropwise condensation, gas liquid equilibria and corrosion processes description. This model takes into account the most important parameters in CO_2 top of the line corrosion: gas temperature, CO_2 partial pressure, gas velocity, condensation rate and HAc concentration. All these effects are described by mathematical equations which are firmly based on the physics behind the processes involved. The model can predict the dropwise condensation rate and the evolvement of the uniform corrosion rate with time.

- Through comparisons with long term experiments, the model shows reasonable performance in prediction of general corrosion rate at top of the line.

ACKNOWLEDGEMENTS

Research for this project is supported by BP, ConocoPhillips, ENI and Total. The authors acknowledge these companies for their technical and financial support and the permission to present the results.

REFERENCES

1. M. Estavoyer, "Corrosion problems at Lack Sour Gas Field", H_2S Corrosion in Oil and Gas production", (Houston, TX; NACE, 1981), p. 905,
2. S. Olsen, A. Dugstad, "Corrosion under Dewing Conditions", CORROSION/91, Paper No. 472 (Houston, TX; NACE, 1991)
3. C. de Waard, U. Lotz, "Prediction of CO_2 Corrosion of Carbon Steel", CORROSION /93, Paper no. 69 (Houston, TX; NACE, 1993)
4. Y. M. Gunaltun, D. Supriyataman, A. Jumaludin, "Top of the Line Corrosion in Multiphase Gas Lines: A Case History", CORROSION /99, Paper No. 36 (Houston, TX; NACE, 1999)
5. B. F. M. Pots, and E. L. J. A. Hendriksen, "CO_2 Corrosion under Scaling Conditions the Special Case of Top-of-the-Line Corrosion in Wet Gas Pipelines", CORROSION/2000, Paper No. 31(Houston, TX; NACE, 2000)
6. F. Vitse, S. Nesic, Y. Gunaltun, "Semi-empirical Model for Prediction of the Top-Of-the-Line Corrosion Risk", CORROSION /2002, Paper No. 2245 (Houston, TX; NACE, 2002)
7. F. Vitse, S. Nesic, Y. Gunaltun, "Mechanistic Model for the Prediction of Top-of-the-Line Corrosion Risk", Corrosion (2003), p. 1075-1084
8. S. Nesic, J. Postlethwite, and S. Olsen, "An Electrochemical Model for Prediction of Corrosion of Mild Steel in Aqueous Carbon Dioxide Solution", Corrosion (1996), p. 280-294
9. M. Nordsveen, S. Nesic and R. Nyborg, "A Mechanistic Model for Carbon Dioxide Corrosion of Mild Steel in the Presence of Protective Iron Carbonate Films - Part 1: Theory and Verification", Corrosion (2003), p. 443-456,
10. S. Nesic, KLJ. Lee, "A Mechanistic Model for Carbon Dioxide Corrosion of Mild Steel in the Presence of Protective Iron Carbonate Films - Part 3: Film growth model", Corrosion (2003), p. 616-628, 2003

11. J.W. Rose, L.R. Glicksman, “Dropwise Condensation: the Distribution of Drop Sizes”, International Journal of Heat Mass Transfer (1973). p. 411-425
12. J.W. Rose, “Some Aspects of Condensation Heat Transfer Theory”, International Communication Heat Mass Transfer (1988), p. 449-473
13. M. Abu-Orabi, “Modeling of Heat Transfer in Dropwise Condensation,” International Journal of Heat Mass Transfer (1998), p. 81-87
14. C. Graham, and P. Griffith, “Drop Size Distributions and Heat transfer in Dropwise Condensation”, International Journal of Heat Mass Transfer (1973), p. 337-346
15. F. W. Dittus, L. M. K. Boetler, University of California at Berkeley, Public Engineering (1930), Vol 2: p. 443-447
16. K. Stephan, Heat Transfer in Condensation and Boiling (Springer-Verlag, 1992), p. 84
17. F. M. White, Fluid Mechanics (McGRAW-HILL International, 1999), p. 460, 4th Edition
18. J. J. Bikerman, “Sliding of Drops from Surfaces of Different Roughness”, Journal of Colloid Science (1950), p. 349-359
19. J. J. Bikerman, Physical Surfaces (Academic Press, 1970), p. 278
20. A. W. Adamson, Physical Chemistry of Surfaces, (John Wiley & Sons, 1990), p. 21
21. E.W. J. van Hunnik, B. F. M. Pots, E. L. J. A. Hendriken, “ The Formation of Protective FeCO3 Corrosion Product Layer in CO_2 Corrosion”, CORROSION /96, Paper No. 6, (Houston, TX; NACE, 1996)
22. C. Mendez, M. Singer, A. Camacho, S. Hernandez, S. Nesic, Y. Gunaltun, M. Joosten, Y. Sun, P. Gabetta, “Effect of Acetic Acid, pH and MEG on the CO_2 Top of the Line Corrosion”, CORROSION /2005, Paper No. 05278, (Houston, TX; NACE, 2005)
23. M. Singer, B. Brown, Z. Zhang, A. Camacho, D. Hinkson, S. Nesic, An unpublished report at Institute for Corrosion and Multiphase Technology (2006)

Table 1**:** Test conditions in large scale loop

Variable parameters		
	Range	
	Min	Max
Absolute pressure (bar)	3	8
pCO_2 (bar)	0.13	8
Gas temperature (°C)	40	90
Condensation rate (mL/m^2/s)	0.05	1
Gas velocity (m/s)	5	15
Free HAc concentration in the tank (ppm)	0	1000
Constant parameters		
Steel type	API X65	
Liquid phase composition	DI water	
pH (tank)	4	
Glycol, methanol, inhibitor content (ppm)	0	
Test duration (weeks)	3	
Internal diameter of pipe (inches)	4	

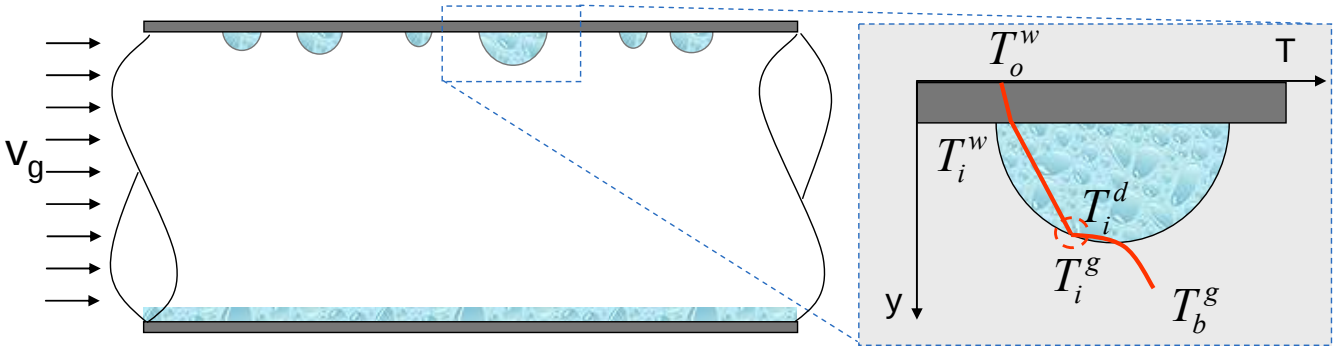

Figure 1 - Temperature gradient in a single droplet. T_o^w : outer wall temperature; T_i^w : inner wall temperature; T_i^d : interfacial temperature in the liquid side; T_i^g : interfacial temperature in the gas side; T_b^g : bulk gas temperature; V_g : gas velocity

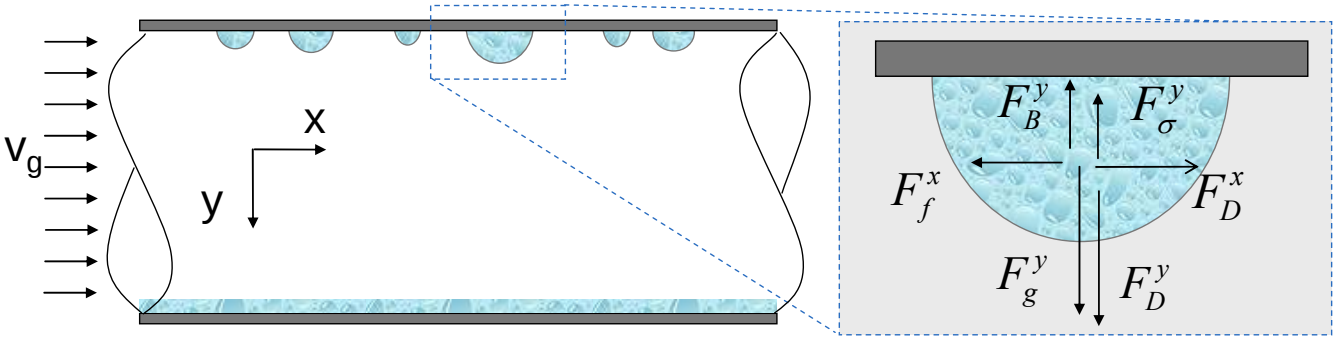

Figure 2 - Force analysis on a single droplet. F_p^y : gas pressure force; F_σ^y : surface tension forece; F_g^y : gravity force; F_D^y : flow drag force in y direction; F_f^x : friction force between the liquid droplet and the solid wall; F_D^x : flow drag force in x direction; V_g : gas velocity

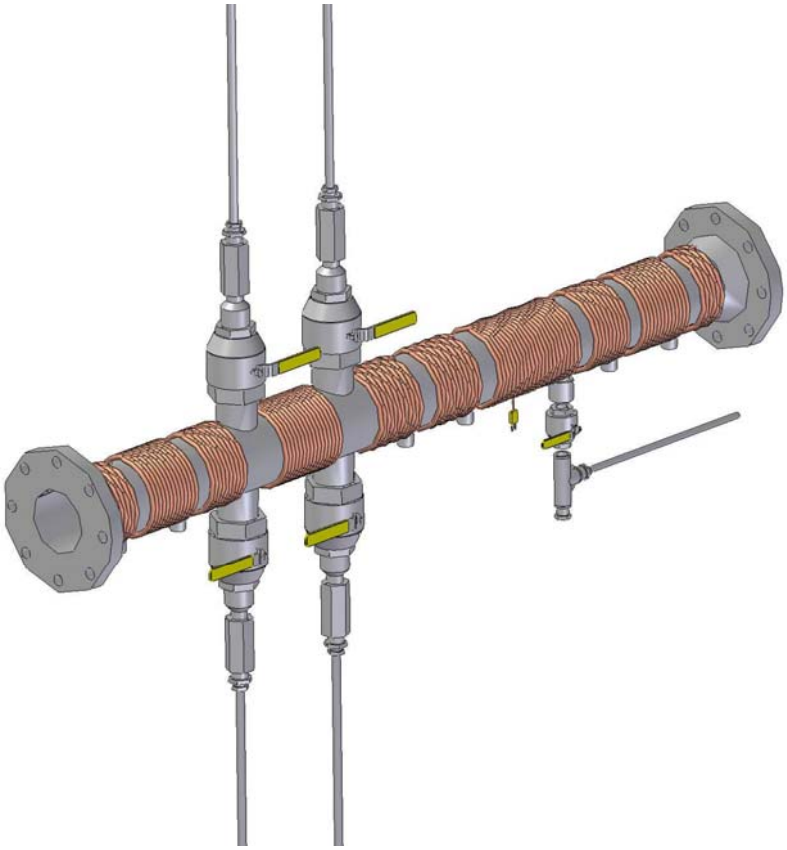

Figure 3 Schematic of the test section in flow loops

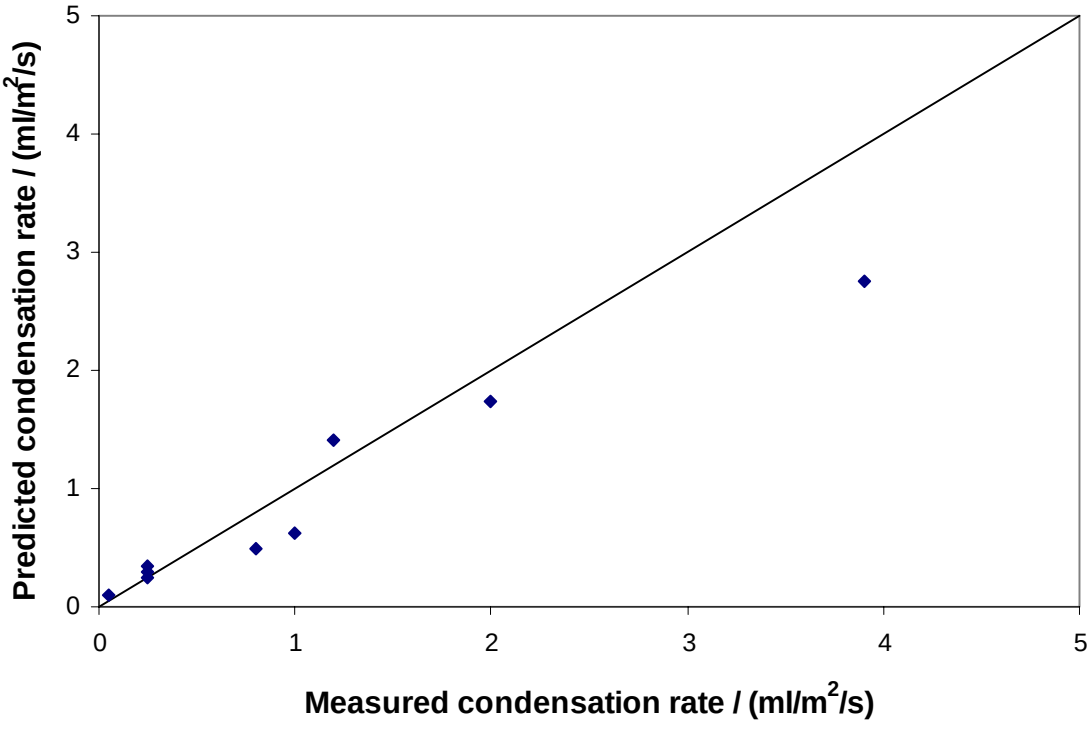

Figure 4 - Comparison of measured and predicted condensation rate

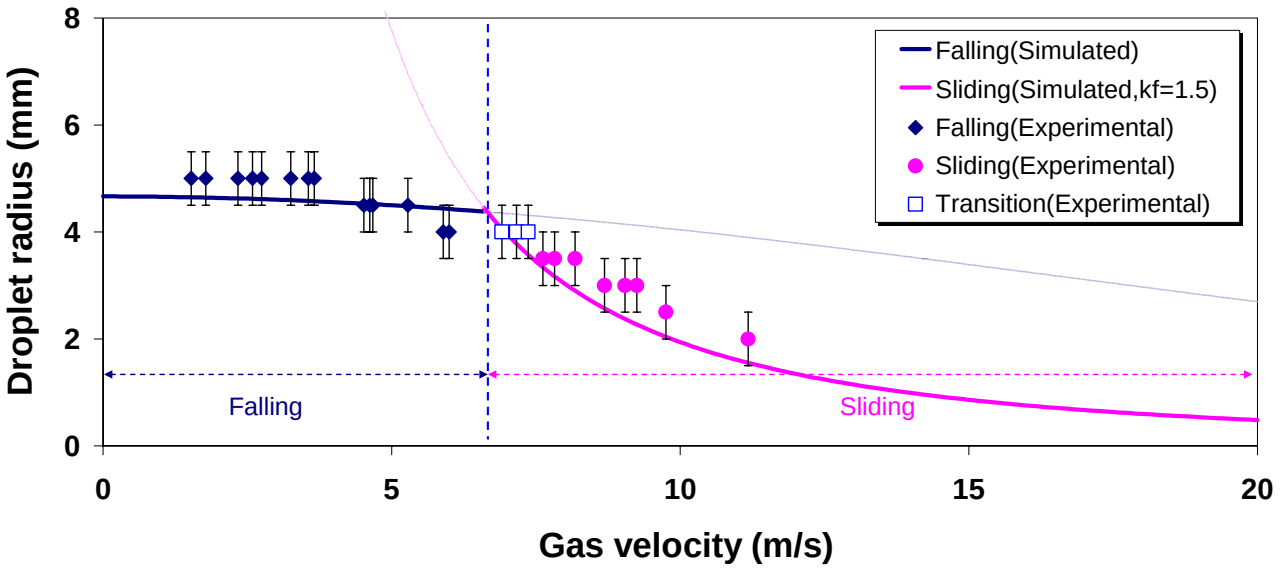

Figure 5 - The transition between sliding droplets and falling droplets,(T_g = 25 ◦C, P_T = 1 bar, k_f =1.5)

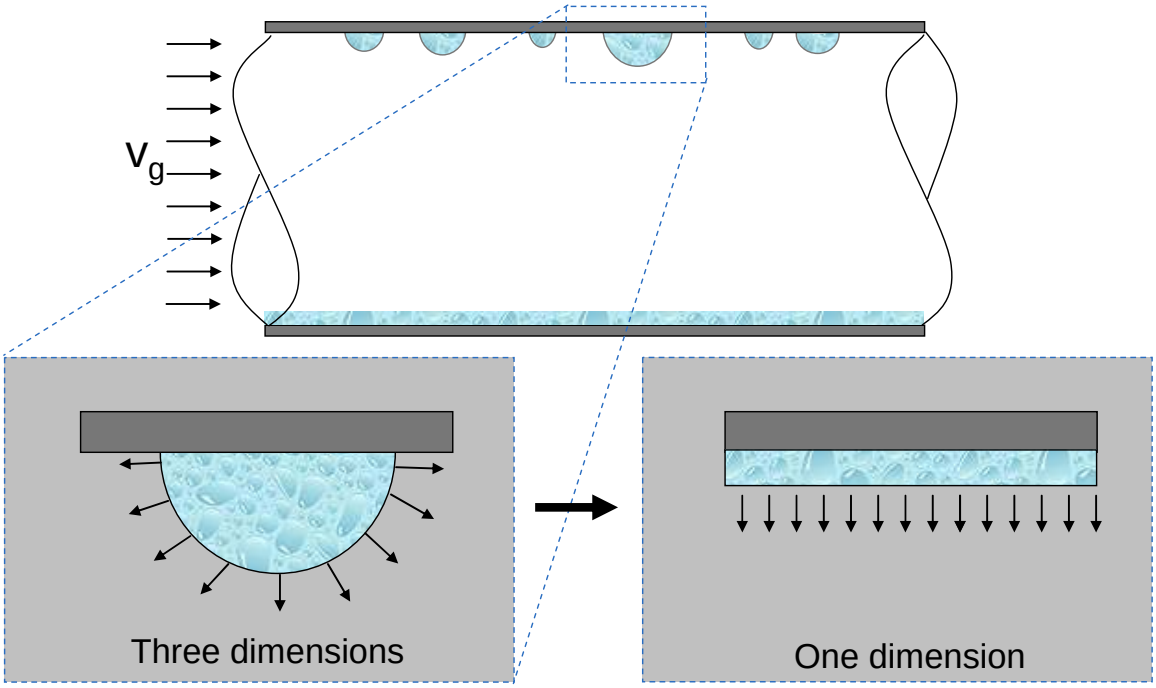

Figure 6 - The simplification from a three-dimension problem to a one dimensional problem

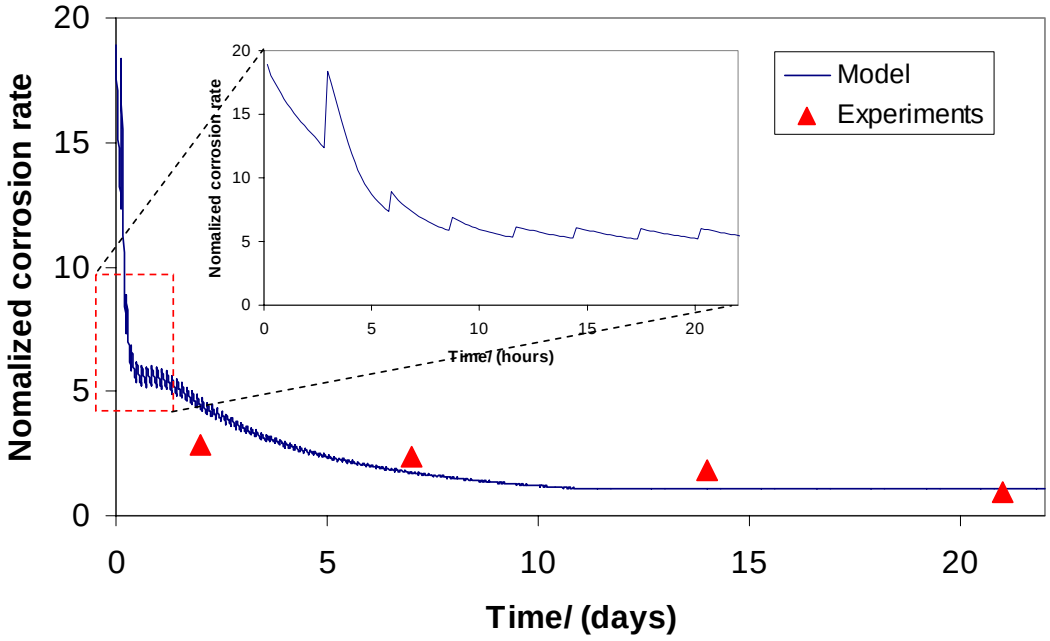

Figure 7 - The comparison between the model and long term experiments (T_g = 70 °C, V_g = 5 m/s, P_T = 3 bar, pCO_2 = 2 bar, Condensation rate = 0.00025 kg/m^2/s)

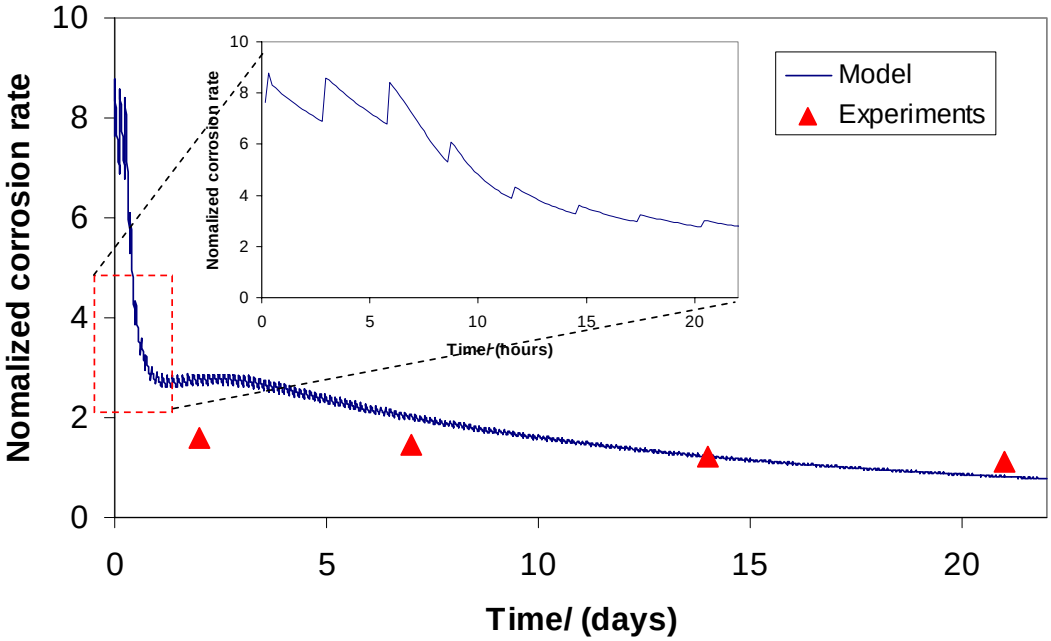

Figure 8 - The comparison between the model and long term experiments (T_g = 40 °C, V_g = 5 m/s, P_T = 3 bar, pCO_2 = 2 bar, Condensation rate = 0.00025 kg/m^2/s)

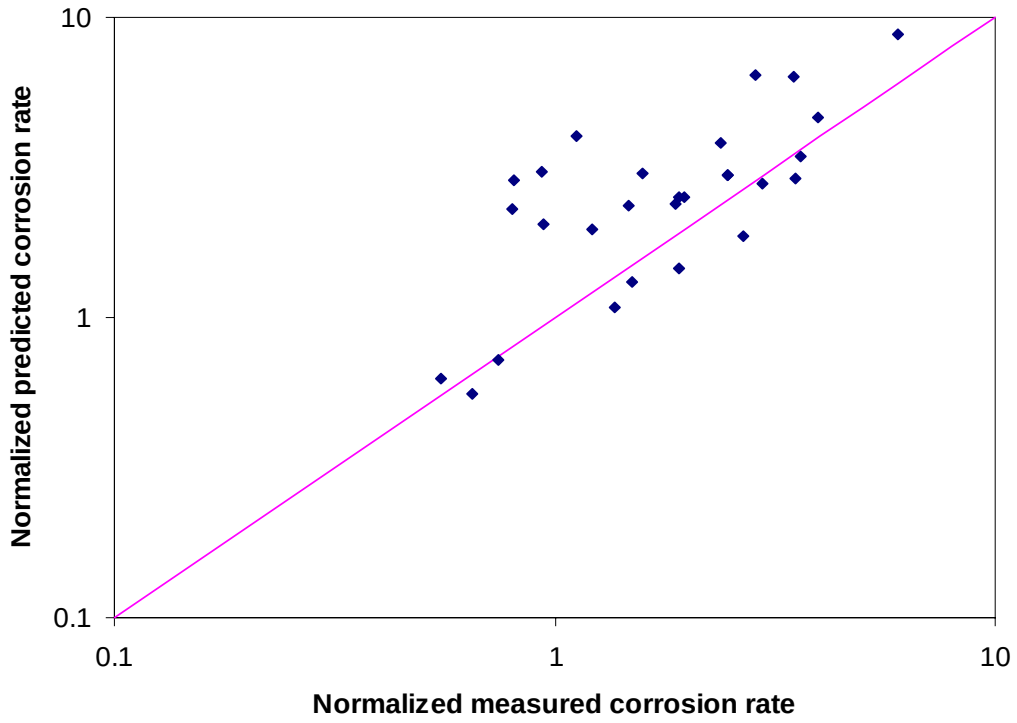

Figure 9 - The comparison between experimental data and predicted results